Supporting Information

Surface-Enhancement in Ultrafast 2D ATR IR Spectroscopy at the Metal-Liquid Interface

Jan Philip Kraack[1‡], Andres Kaech[2], and Peter Hamm[1┼]

[1]Department of Chemistry, University of Zürich,

Winterthurerstrasse 190, CH-8057, Zürich, Switzerland

[2]Center for Microscopy and Image Analysis, University of Zürich,

Winterthurerstrasse 190, CH-8057, Zürich, Switzerland.

Dependence of Au Plasmon Resonance Absorption Spectra on Average Metal Thickness

The enhancement effect in ATR IR spectroscopy is explained using the polarization of metal nanoparticles (NPS) and the off-resonant excitation of local surface plasmon (LSP) resonances which stem from structured metal surfaces (see Fig. 4 in the main text and Fig. SI 3 below).[1,2] Au NPs exhibit pronounced LSP resonances with dominant absorption in the spectral region between 500 – 800 nm. This is demonstrated here by recording broadband absorption spectra from sputter-coated CaF_2 substrates of varying average thicknesses in a stationary UV-Vis spectrometer. As depicted in Fig. SI 1, the peak LSP resonance of the Au NPs is located at about 580 nm for 0.2 nm Au, strongly broadens and red-shifts with increasing average thickness to about 660 nm. This is indicative for a growth of the Au NPs on the prisms surface as the average sputtered thickness increases.[3,4]

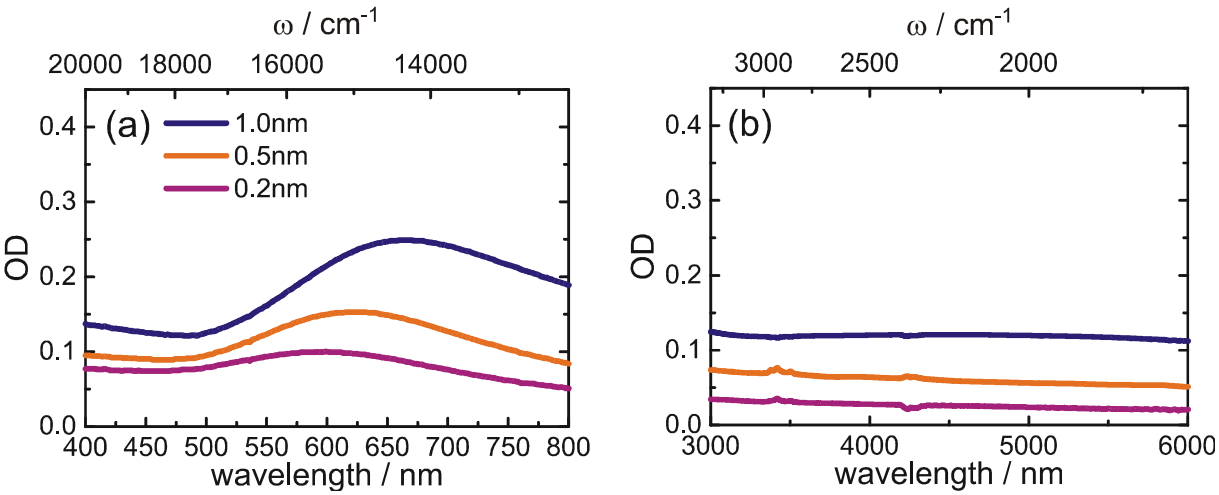

Fig. SI 1. Surface plasmon resonance spectra recorded from sputtered ultrathin Au layers between 0.2 nm and 1.0 nm. (a) Stationary UV-Vis absorption spectra from Au on CaF_2. (b) Stationary ATR IR spectra of Au on ZrO_2.

Calculation of the x, y, and z-Components of the Evanescent Wave in the CaF_2-MeOH System

As discussed in the main text, p- and s-polarization of the incident light induce differently polarized evanescent waves at the solid-liquid interface in ATR IR spectroscopy.[5] That is, p-polarized incident light generates an elliptically polarized evanescent wave in the optically-rarer medium (here: MeOH). Here, the evanescent wave exhibits a major z-component (for definitions, see Figs. 1 and 3 in the main text) and a minor x-component as evidenced for a projection of a temporal oscillation of the evanescent wave in the x-z-plane (Fig. SI 2 (a)). Conversely, s-polarization generates a linearly polarized evanescent wave in the optically rarer medium with only a y-component (Fig. SI 2 (b)) for a projection of a temporal oscillation of the evanescent wave in the x-y-plane.

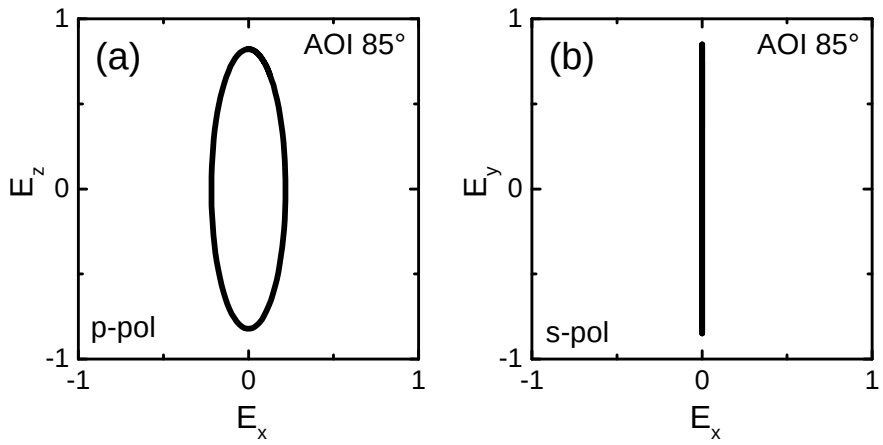

Figure SI 2. Calculation of the x, y, and z-components of the evanescent wave at the CaF_2-MeOH interface. Shown are the projections of a temporal oscillation of the electric field vector to indicated planes for (a) p-polarized incident light and (b) s-polarized incident light.

Large Scale SEM Images from Au-coated and non-Au-coated CaF_2 Substrates

The main text discusses SEM images of Au sputter-coated and non-Au coated CaF_2 substrates in terms of the structure of the corresponding Au NPs. Here we show large range SEM images of the same substrates in order to allow for a better comparison of the surface structure (Fig. SI 3). The order of the images is the same as in the main text, *i.e.* 0.2 nm Au (a), 0.5 nm Au (b), 1.0 nm Au (c), and no Au (d). The growing size of the Au NPs with increasing average thickness and the formation of pronounced gaps between the NPs can be discerned.

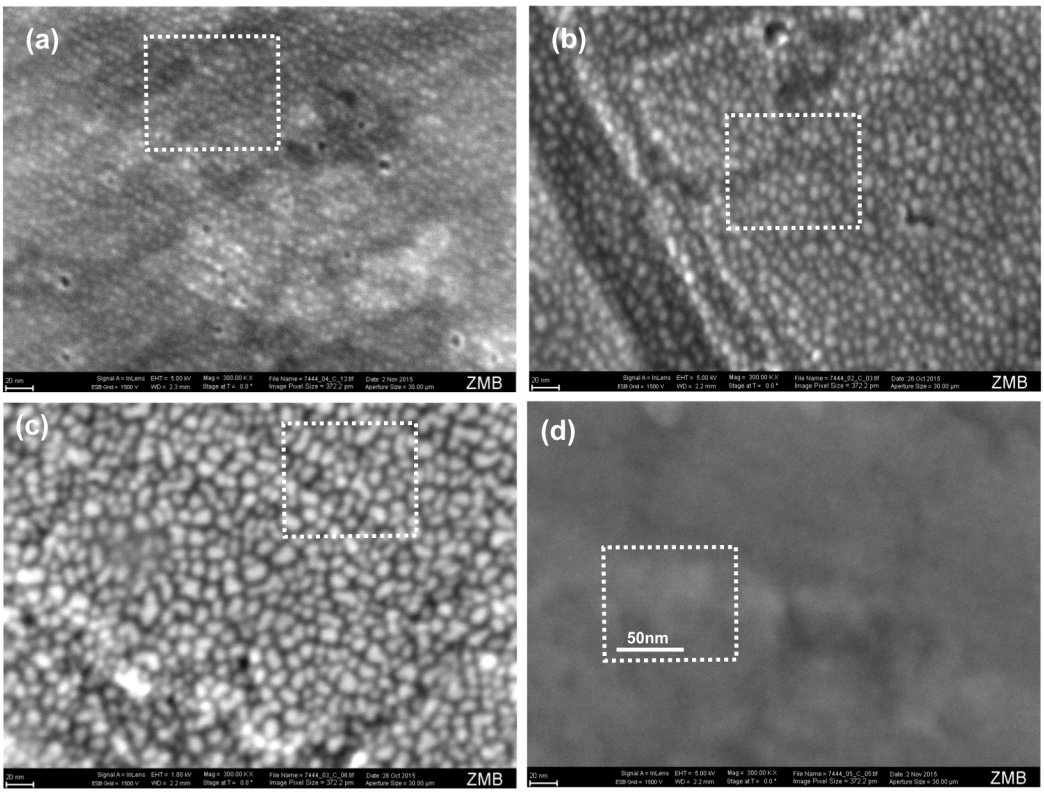

Figure SI 3. Large Scale SEM images of CaF_2 substrates which have been sputter-coated with (a) 0.2 nm Au, (b) 0.5 nm Au, and (c) 1.0 nm Au. (d) Shows an SEM image of a non-Au-coated CaF_2 substrate. Note that all substrates have been additionally coated with 2 nm of Carbon in order to allow for high enough conductivity which allows a high-resolution SEM analysis. Regions of white dashed margins correspond to the excerpts shown in the main text (Fig. 4). All images have been acquired with an acceleration voltage of 5 kV and the magnification (300 k) leads to an image pixel size of 372.2 pm.

Vibrational Relaxation Dynamics of Samples

Vibrational relaxation can influence the values of EFs for delays other than T = 0 ps if relaxation time constants drastically differ. Here, we show that the calculation of EFs is only minimally influenced through vibrational relaxation for the sample systems investigated here. Fig. SI 4 shows 2D ATR IR signal magnitudes for p-PhCN and 2N3 for both bulk solution as well as ML data. Symbols represent experimental data of bulk solution samples (black) and ML samples (red), while solid lines represent exponential fits (same color code). For p-PhCN (Fig. SI 4 (a)) dissolved in (bulk) or incubated with (ML) MeOH, vibrational relaxation takes place with time constants of 7.6 ± 0.3 ps (bulk) and 8.0 ± 0.2 ps. Which indicates negligible influence of vibrational relaxation on EFs for calculation of EFs at 5 ps as done in the main text. Fig. SI 4 (b) shows the same data for 2N3 bulk solution and ML relaxation dynamics. Exponential fits to the data yield time constants for vibrational relaxation of 1.3 ± 0.1 ps (bulk) and 1.7 ± 0.1 ps (ML). This slight difference in the vibrational relaxation time constants would yield for a population delay of 1 ps (in the absence of any enhancement effects discussed in the main text) an EF for the ML sample of 1.2. This is thus significantly lower as the experimentally observed value for 2N3 on 1 nm Au (EF ≈ 7).

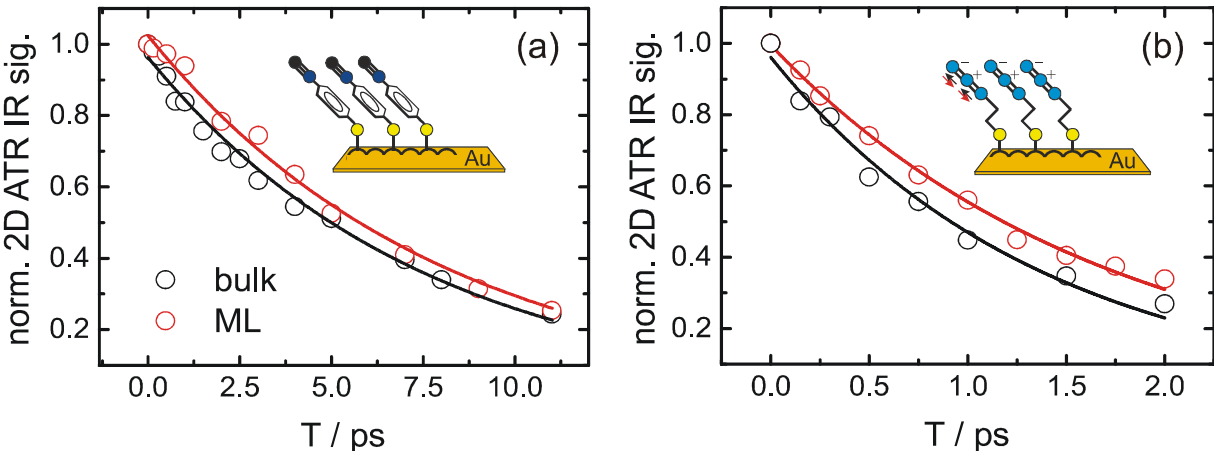

Figure SI 4. Vibrational relaxation of (a) p-PhCN and (b) 2N3 for bulk solution samples (black) and ML samples (red). Experimental data are represented by symbols while exponential fits are represented by solid lines.

Enhancement Factors for Aliphatic Nitrile Functional Groups

The main text discusses the previously observed influence of polarity and polarizability in surface-enhanced IR signals.[1,6–10] Here we show that the polarity and polarizability of the two different employed vibrational probes (azide and nitrile) *per se* have a negligible influence on the EFs of aliphatic MLs on Au in 2D ATR IR spectroscopy.[11–14] Fig. SI 5 (a) shows ATR IR absorption spectra of 4-Cyanobutanethiol (4CN) dissolved in bulk MeOH (black) as well as for 4CN MLs on 1 nm Au on CaF_2 under the same experimental conditions as for the other ML samples in the main text. Fig. SI 5 (b) shows the corresponding diagonal cuts of the 2D ATR IR spectra. A relation of the obtained signal magnitudes according to eqn. (1) in the main text reveals an EF of 7. This demonstrates that the signal enhancement for the aliphatic nitrile and azide containing ML samples is similar.

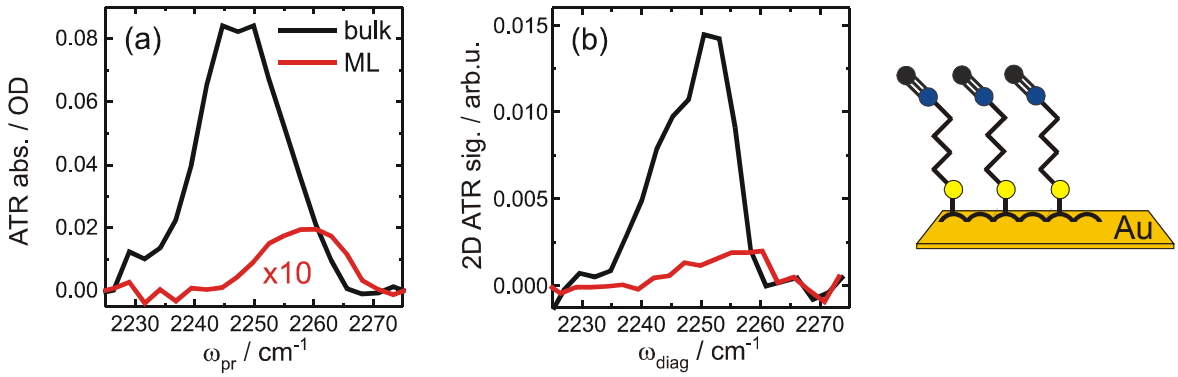

Figure SI 5. Determination of the EF for 4-Cyanobutanethiol (4CN) MLs on 1 nm Au in 2D ATR IR spectroscopy. (a) ATR IR absorption spectra of 4CN in bulk MeOH (black) and as MeOH-incubated MLs (red). (b) Corresponding diagonal cuts of the 2D ATR IR spectra at a population delay of 1 ps. The calculated EF is ≈ 7. To the right is a sketch of the ML sample.

Enhancement Factors for Aromatic Azide Functional Groups

Figs. 2 and 5 in the main text together with Fig. SI 5 show that aromatic samples exhibit different EFs as compared to aliphatic samples. This trend is further supported here by the determination of EFs for aromatic azide functional groups in para-Azidophenyl-isothiocyanate (p-PhN3) MLs on 1 nm Au. Fig. SI 6 (a) shows ATR IR absorption spectra of p-PhN3 dissolved in bulk MeOH (black) as well as for p-PhN3 MLs on 1 nm Au on CaF_2 under the same experimental conditions as for the other ML samples in the main text. Fig. SI 6 (b) shows the corresponding diagonal cuts of the 2D ATR IR spectra. A relation of the obtained signal magnitudes according to eqn. (1) in the main text reveals an EF of 24. This demonstrates that the signal enhancement for the aromatic ML samples is similar and in general stronger than enhancement of aliphatic MLs, irrespective of the functional group.

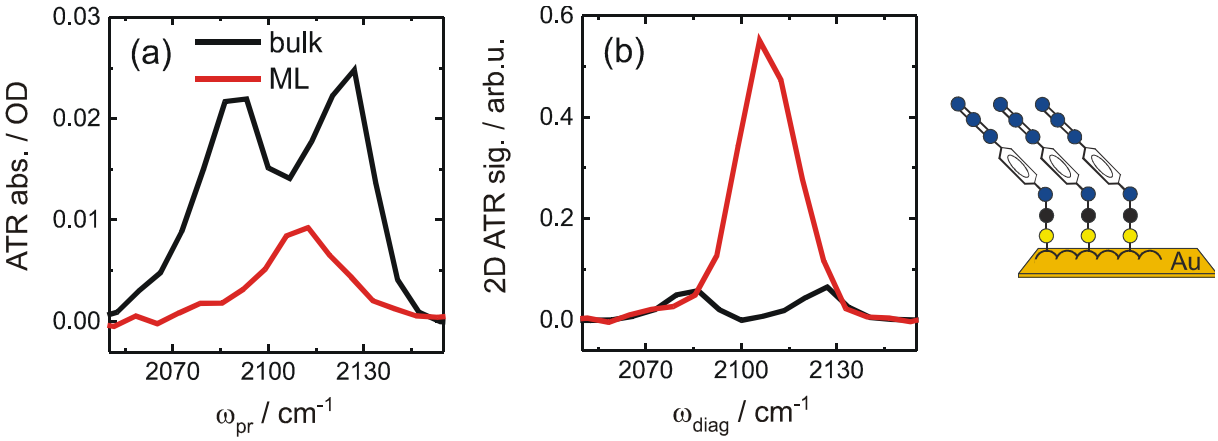

Figure SI 6. Determination of the EF for para-Azidophenyl-isothiocyanate (p-PhN3) MLs on 1 nm Au in 2D ATR IR spectroscopy. (a) ATR IR absorption spectra of PhN3 in bulk MeOH (black) and as MeOH-incubated MLs (red). (b) Corresponding diagonal cuts of the 2D ATR IR spectra at a population delay of 0.1 ps. The calculated EF is ≈ 24. To the right is a sketch of the ML sample.

Note that for p-PhN3 the bulk solution sample exhibits two peaks which may arise from intramolecular coupling between the SCN functional group and the N_3-label. Interestingly, the

double band structure is abrogated for the ML sample and a single peak is observed both in the stationary signals as well as in the 2D ATR IR data. Due to the exploitation of the SCN group as a linker to the Au surface, it can be expected that the vibrational properties of the linker group are significantly affected through the adsorption process. This may eliminate vibrational coupling between the two functional groups.

Note additionally, that p-PhN3 is linked to the Au layers via an isothiocyanate functional group as compared to the thiol-linkers for 4CN, 2N3 and the PhCN compounds in the main text. Therefore, the lower increase in enhancement for p-PhN3 as compared to 2N3 might be reasoned by different conformational arrangements of the two ML samples based on the different linkers in the two systems.

References

(1) Osawa, M. Surface-Enhanced Infrared Absorption. In *Near-Field Optics and Surface Plasmon Polaritons*; S. Kawata, Ed.; Springer-Verlag Berlin Heidelberg, 2001; Vol. 81, pp. 163–187.

(2) Aroca, R. *Surface-Enhanced Vibrational Spectroscopy*; John Wiley & Sons, Ltd: Chichester, UK, 2006.

(3) Siegel, J.; Lyutakov, O.; Rybka, V.; Kolská, Z.; Svorčík, V. Properties of Gold Nanostructures Sputtered on Glass. *Nanoscale Res. Lett.* **2011**, *6*, 96.

(4) Osawa, M.; Kuramitsu, M.; Hatta, A.; Suetaka, W. Electromagnetic Effect in Enhanced Infrared Absorption of Adsorbed Molecules on Thin Metal Films. *Surf. Sci. Lett.* **1986**, *175*, L787–L793.

(5) Kaneko, F.; Miyamoto, H.; Kobayashi, M. Polarized Infrared Attenuated Total Reflection Spectroscopy for Three-Dimensional Structural Analysis on Long-Chain Compounds. *J. Chem. Phys.* **1996**, *105*, 4812.

(6) Osawa, M.; Ikeda, M. Surface-Enhanced Infrared Absorptlon of P -Nitrobenzole Acid Deposited on Silver Island Fllms : Contributions of Electromagnetic and Chemical Mechanisms. *J. Phys. Chem.* **1991**, *95*, 9914–9919.

(7) Zhang, Z.; Imae, T. Study of Surface-Enhanced Infrared Spectroscopy. *J. Colloid Interface Sci.* **2001**, *233*, 99–106.

(8) Badilescu, S.; Ashrit, P. V.; Truong, V. V. Enhanced Infrared Attenuated-Total-Reflection Spectra of P-Nitrobenzoic Acid with Ag Films. *Appl. Phys. Lett.* **1988**, *52*, 1551–1553.

(9) Merklin, G. T.; Griffiths, P. R. Influence of Chemical Interactions on the Surface-Enhanced Infrared Absorption Spectrometry of Nitrophenols on Copper and Silver Films. *Langmuir* **1997**, *13*, 6159–6163.

(10) Chen, T.; Borchers, R. L.; Perry, D. A. Surface-Enhanced Infrared Absorption Spectroscopic Investigation of Benzamide Thin-Film Formation, Stability, and Catalysis on Gold and Silver Nanostructures. *Part. Sci. Technol.* **2014**, *32*, 234–241.

(11) Kraack, J. P.; Lotti, D.; Hamm, P. Ultrafast, Multidimensional Attenuated Total Reflectance Spectroscopy of Adsorbates at Metal Surfaces. *J. Phys. Chem. Lett.* **2014**,

5, 2325–2329.

(12) Kraack, J. P.; Lotti, D.; Hamm, P. Surface-Enhanced, Multi-Dimensional Attenuated Total Reflectance Spectroscopy. In *Proc. of SPIE, Physical Chemistry of Interfaces and Nanomaterials XIV*; Sophia C. Hayes; Eric R. Bittner, Eds.; 2015; Vol. 9549, p. 95490S.

(13) Kraack, J. P.; Lotti, D.; Hamm, P. 2D Attenuated Total Reflectance Infrared Spectroscopy Reveals Ultrafast Vibrational Dynamics of Organic Monolayers at Metal-Liquid Interfaces. *J. Chem. Phys.* **2015**, *142*, 212413.

(14) Lotti, D.; Hamm, P.; Kraack, J. P. Surface-Sensitive Spectro-Electrochemistry Using Ultrafast 2D ATR IR Spectroscopy. *J. Phys. Chem. C* **2016**, *accepted*, DOI:10.1021/acs.jpcc.6b00395.